Electrochimica Acta 206 (2016) 301–306

Contents lists available at ScienceDirect

Electrochimica Acta

journal homepage: www.elsevier.com/locate/electacta

One step synthesis of vanadium pentoxide sheets as cathodes for lithium ion batteries

Haoyang Wu[a], Mingli Qin[a,*], Xiaoli Li[a], Zhiqin Cao[a,b], Baorui Jia[a], Zili Zhang[a], Deyin Zhang[a], Xuanhui Qu[a], Alex A. Volinsky[c]

[a] School of Materials Science and Engineering, University of Science and Technology Beijing, Beijing 100083, China
[b] School of Resources and Environmental Engineering, Pan Zhihua University, Pan Zhihua 617000, China
[c] Department of Mechanical Engineering, University of South Florida, E. Fowler Ave., ENB118, Tampa FL 33620, USA

ARTICLE INFO

Article history:
Received 19 December 2015
Received in revised form 26 March 2016
Accepted 28 April 2016
Available online 29 April 2016

Keywords:
vanadium pentoxide
sheets
pyrolysis
cathode

ABSTRACT

Orthorhombic single crystal V_2O_5 sheets with lateral dimensions of 4–6 μm were synthesized by a facile one-pot organics-assisted pyrolysis method. TG-MS measurements revealed the intrinsic reaction mechanism of the as-prepared V_2O_5 sheets. As cathode materials for the lithium ion batteries (LIBs), V_2O_5 sheets delivered high initial discharge capacity of 310 mA h g^{-1} and the coulombic efficiency remained close to 100% during the 50 charge-discharge cycles. Good electrochemical performance is attributed to the unique sheet structure, which increases the contact area between the active material and the electrolyte. Moreover, the structure greatly facilitates intercalation and deintercalation of Li^+ ions and electron transport. Developed approach is simple, low cost and has excellent scalability for preparing V_2O_5 sheets as high-performance LIBs cathodes.

1. Introduction

Vanadium oxides are useful transition metal oxides for plenty of scientific and industrial applications, since vanadium, an abundant element in the Earth crust, has variable oxidation states from +2 to +5 (VO, V_2O_3, VO_2, and V_2O_5) [1]. Vanadium pentoxides (V_2O_5) possess crystal structure formed by stacking V_2O_5 layers perpendicular to the c-axis via van der Waals interactions [2,3], and have been widely studied in the past decades. As a typical intercalation compound, a large variety of atomic and molecular species can be reversibly intercalated and de-intercalated between V_2O_5 layers. Since the mid-1970s, V_2O_5 has been extensively studied as electrode materials in energy storage devices, such as lithium-ion batteries (LIBs) [4–9] and supercapacitors [10–13]. However, the practical application of V_2O_5 has been substantially hindered by the poor kinetics due to intrinsically low diffusion coefficient of lithium ions (10^{-14} to 10^{-12} cm^2 s^{-1}) [14,15] and low electric conductivity (10^{-2} to 10^{-3} S cm^{-1}) [16,17].

Many investigations demonstrated that the structure of V_2O_5 has a significant impact on the electrode-electrolyte contacts, influencing the lithium ion diffusion distance and reversibility of the V_2O_5-based electrodes [5,18,19]. Up to date, V_2O_5 materials with various structures, such as zero-dimensional(0D) particles [20], one-dimensional(1D) tubes/wires/rods [14,21] and two-dimensional(2D) sheets [2,17,22], have been reported, which considerably improved V_2O_5 chances as electrode material. In particular, 2D sheets are the most ideal structures because their unique planar configurations offer shortened diffusion path for lithium ions [23] and more electrochemically active sites, leading to meaningful improvements in these electrochemical electrodes [24].

Previously, several efforts have been made to synthesise V_2O_5 sheets, which include hydrothermal techniques, liquid exfoliation technique, soft template methods, and supercritical solvothermal reactions [2,17,25–27]. In typical examples, Rui et al. [17] have reported synthesis of few-layer V_2O_5 sheets through direct exfoliation of bulk V_2O_5 crystals in formamide solvent. An [25] and coworkers have synthesized V_2O_5 sheets via supercritical solvothermal reaction followed by annealing treatment. These V_2O_5 sheets both displayed larger reversible capacity, higher coulombic efficiency, and more stable cyclability than bulk V_2O_5 powders. However, these processes usually consist of complicated procedures, including a long-term aging reaction, ethanol immersing process, repeated washing and heating at different stages to obtain the final product. Apparently, development of a simple synthesis route with excellent scalability and low cost should be

* Corresponding author. Tel.: +86 10 82375859; fax: +86 10 62334311.
E-mail address: qinml@mater.ustb.edu.cn (M. Qin).

http://dx.doi.org/10.1016/j.electacta.2016.04.169
0013-4686/

addressed for meeting practical applications. In this paper, we present a unique approach for synthesizing V_2O_5 sheets by developing a chemical reaction using an organics-assisted pyrolysis process. In contrast to conventional synthetic processes, this one-step method possesses various advantages of simple process, low cost and easy scalability. Electrochemical characterizations suggest the as-prepared V_2O_5 sheets hold great potential as the promising low-cost cathode materials in the LIB.

2. Experimental

In the synthesis process, ammonium metavanadate (NH_4VO_3) (0.05 M) acted as vanadium source and ammonium nitrate (NH_4NO_3) and urea ($CO(NH_2)_2$) (molar ratio of NH_4NO_3 to CO $(NH_2)_2$ of about 8) were the organic agents. A precursor solution was prepared by dissolving all reactants in a sufficient amount of water. During the experiments, the ratio between urea and ammonium metavanadate, ϕ, was in the range from 0.5 to 7. Upon heating, clear yellow solution was gradually changed to the yellowish powders with the solution evaporation. For comparison, the reactions (ϕ = 7) that without adding NH_4NO_3 or $CO(NH_2)_2$ were named VU1 and VU2, respectively.

Thermogravimetric differential scanning calorimeter (TGA-DSC) device (NETZSCH-Gerätebau GmbH, Germany) coupled with a mass spectrometer (QMS403C) is used to perform in situ thermogravimetric and gas-phase analysis of reactive gels during the reaction process. Phases of the powders were investigated by X-ray diffraction (XRD, MXP21VAHF) at room temperature. Morphology of the powders was characterized by scanning electron microscopy (SEM, JSM-6510) and transmission electron microscopy (TEM, Tecnai G2 F30 S-TWIN). X-ray photoelectron spectra (XPS) were recorded with an ESCALAB 250 spectrometer (PerkinElmer) to characterize the surface composition.

Electrochemical measurements were performed in the CR2023-type coin cells. The electrode (working electrode) was fabricated by mixing the active materials with acetylene black and a binder, poly (vinylidene fluoride), at weight ratio of 80:10:10. The mixture was dispersed in the N-methylpyrrolidone solvent to form slurry and uniformly pasted on the Al foil with a blade. These prepared electrode sheets were dried at 120 °C in a vacuum oven for 12 h and pressed under the 200 kg m^{-2} pressure. The CR2032-type coin cells were assembled in a glove box for electrochemical characterization. A non-aqueous solution of 1 M $LiPF_6$ in a 1:1 ethylene carbonate (EC) and dimethyl carbonate (DMC) was used as electrolyte. Li metal disk was used as the counter electrode for electrochemical testing. The cells were galvanostatically charged and discharged in a current density range of 29.4 mA g^{-1} (0.1C) within the 2–4 V voltage range. For the high rate testing, the charge/discharge current gradually increased from 0.1C to 0.2, 0.5, 1, and 2C, and then decreased to 0.2C, step by step. Cyclic voltammetry (CV) curves were collected using an electrochemistry workstation (CHI618D) at 0.2 mV s^{-1} in the 2.0-4.0 V range.

3. Results and Discussion

XRD patterns of the three powders are shown in Fig. 1 (a). At ϕ = 0.5, the reaction leads to the formation of $(NH_4)_2V_6O_{16}$ and NH_4NO_3, indicating that the pyrolysis procedure was inadequate. With the increase of the ratio ϕ to 7, all the peaks could be indexed to the crystalline orthorhombic V_2O_5 phase (JCPDS 85-0601) and no other purity peaks were observed.

The SEM images (Fig. 2(a)) of the sample (ϕ = 0.5) Exhibits 2D sheet structure. With an increasing amount of urea, both the thickness and lateral dimensions decrease. The pure V_2O_5 (ϕ = 7) consists of sheets with 4–6 μm lateral dimensions. The TEM image (Fig. 2(d)) clearly reveals that the sheet morphology of the V_2O_5

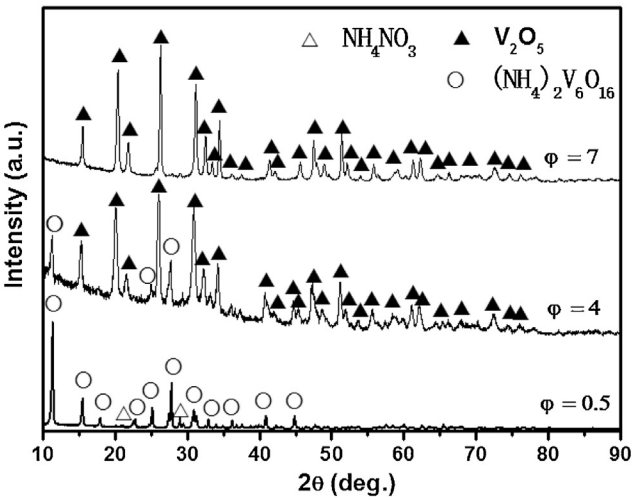

Fig. 1. XRD pattern of the three powders.

(ϕ = 7).The HRTEM image (Fig. 2(e)) shows clear lattice fringes with a spacing of 0.34 nm, corresponding with the distance of (110) planes quite well. The selected area electron diffraction (SAED) patterns from an individual V_2O_5 sheet (insert in Fig. 2(d)) show the single crystalline nature of the individual V_2O_5 sheet.

For understanding the formation of V_2O_5 sheets during the synthesis process, this reaction was characterized by TG-DSC coupled with a mass spectrometer (MS). In contrast, calcination of ammonium metavanadate was characterized in air by the same methods. These experiments were carried out from room temperature to 400 °C at a heating rate of 10 °C·min^{-1} in air. Fig. 3(a) shows calcination of the NH_4VO_3 powders with ~180 °C initial temperature, and three endothermic peaks can be observed in the 50–400 °C temperature range. The average weight losses were about 15.45%, 1.84% and 4.51% for the first, second and third step, respectively, consistent with the observation in another study [29]. In the work by Tang et al. [29], the observed NH_4VO_3 mass loss is due to the vaporization of physically absorbed water and decomposition of NH_4VO_3, coupled with a large amount of gases (NH_3, H_2O, NO, and etc.) generated simultaneously. As shown in Fig. 3(b), the calcined product is comprised of bulk V_2O_5. The related reactions are presented as follows

$$2NH_4VO_3 \rightarrow V_2O_5 + 2NH_3 + H_2O \quad (1)$$

$$4NH_3 + 7O_2 \rightarrow 4NO_2 + 6H_2O \quad (2)$$

$$4NH_3 + 5O_2 \rightarrow 4NO + 6H_2O \quad (3)$$

Fig. 3(c) and (d) show the TG-DSC-MS data of the reaction (ϕ = 7). Only endothermic peaks are observed during the procedure, confirming the presence of pyrolytic reaction. At the initial stage (below 150 °C), the presence of a small endothermic peak, accompanied with ~17% weight loss, is attributed to vaporization of chemically absorbed water and decomposition of NH_4NO_3, resulting in the formation of H_2O and NH_3 gases (as shown in Fig. 3(d)). In the second stage, the sharp weight loss with two huge endothermic peaks occurring around 230 °C and 285 °C were caused by the pyrolytic reaction of the gel. The gases released during the fast process contained NH_3, H_2O, NO, NO_2 and CO_2, which also can be confirmed by Fig. 3(d). For comparison, the reactions (VU1 and VU2) have been prepared. As shown in the TG-DSC data (Fig.S1), the synthesis process of VU1 actually is an exothermic reaction. Although the synthesis process of VU2 is also

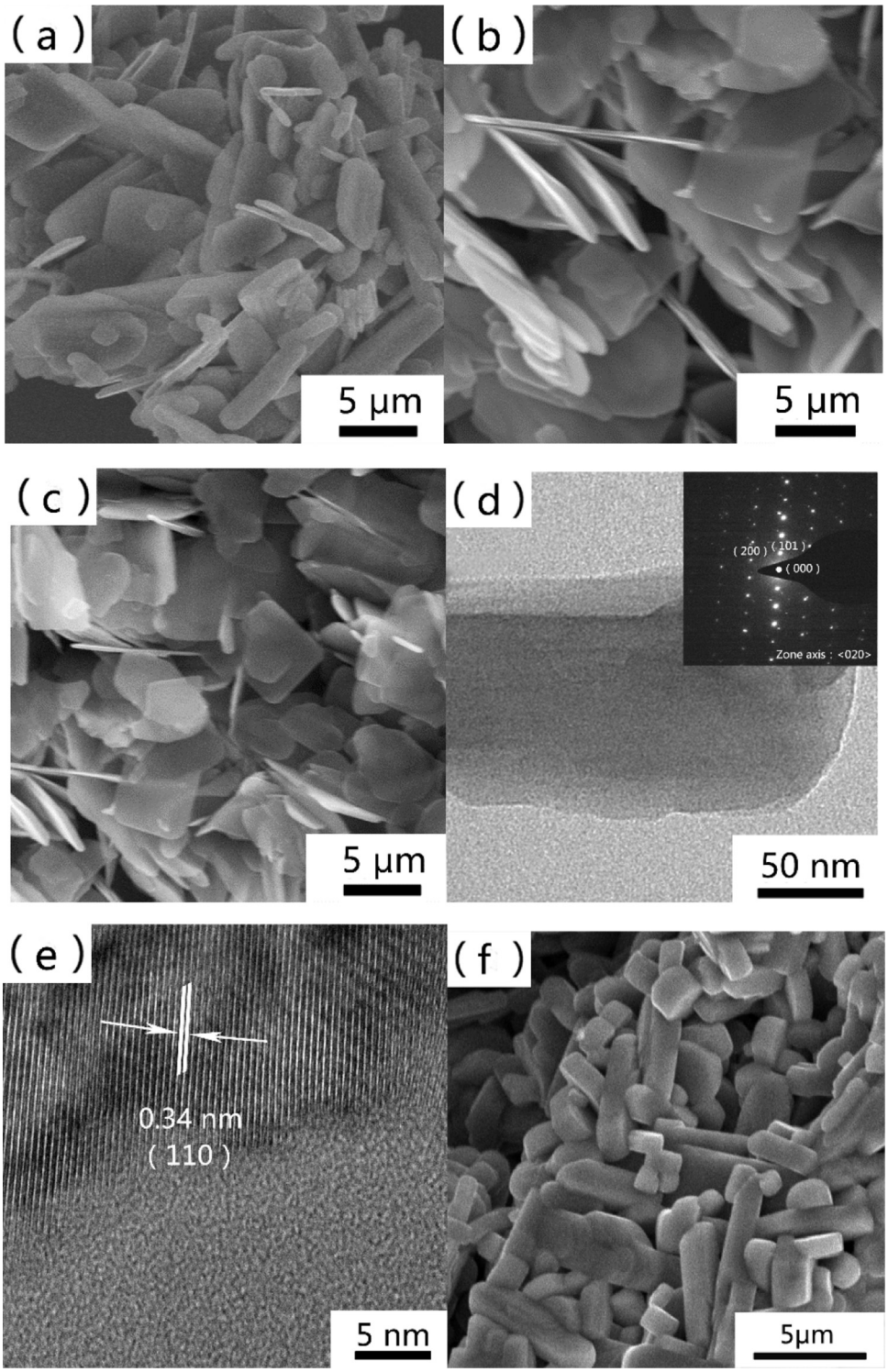

Fig. 2. (a), (b) and (c) SEM images of three products (ϕ = 0.5, 4 and 7), (d) HRTEM image (SAED patterns in inset) and (e) HRTEM image of orthorhombic V_2O_5 sheets (ϕ = 7); (f) SEM image of bulk V_2O_5 synthesised by calcination of NH_4VO_3.

a pyrolytic reaction, the reaction leads to the formation of $(NH_4)_2V_6O_{16}$, NH_4NO_3 and V_2O_5 irregular blocks (Fig. S2 and S3). Fig.S4 shows the FTIR spectra of all the raw materials and gelatinous mass. In the gelatinous mass(ϕ = 7), some characteristic peaks of raw materials have disappeared and new peaks occur compared with other samples. The above phenomena indicate that the three raw materials coordinate with each other and form new complex gelatinous mass during the second stage(ϕ = 7). Although the exact mechanism of synthesizing single crystal V_2O_5 sheets needs further investigations, the coordination effects of the three raw materials should be an important part[30–32]. The overall evolutionary illustrations of the V_2O_5 sheets are shown in Fig. 4. The related reactions are presented as follows.

$$14NH_4NO_3 + 2NH_4VO_3 + CO(NH_2)_2 \rightarrow 16NO_2 + CO_2 + V_2O_5 + 16NH_3 + 10H_2O \quad (4)$$

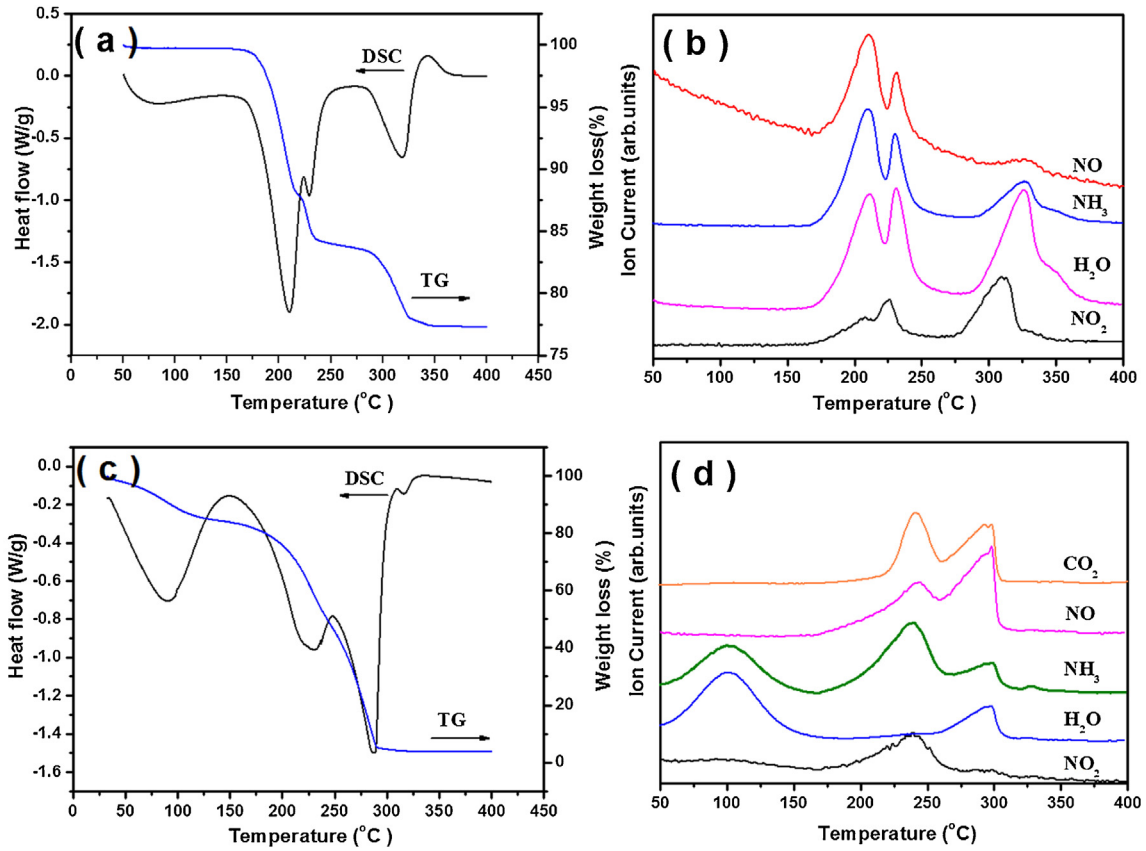

Fig. 3. Results of TG–DSC and MS analysis for the synthesis process of bulk V_2O_5 ((a) and (b)) and V_2O_5 sheets ((c) and (d)).

$$10NH_4NO_3 + 2NH_4VO_3 + 3CO(NH_2)_2 \rightarrow 16NO + 3CO_2 + V_2O_5 + 12NH_3 + 12H_2O \quad (5)$$

The as-prepared 2D V_2O_5 sheets were utilized as cathode materials for LIBs. Fig. 5a shows the typical cyclic voltammograms (CVs) of the V_2O_5 sheets in the voltage window of 2–4 V vs. Li/Li^+ at a scan rate of 0.2 mV s^{-1}. The following equation indicates typical intercalation mechanism in V_2O_5 matrix.

$$V_2O_5 + xLi^+ + xe^- \leftrightarrow Li_xV_2O_5 \quad (6)$$

As a result, the two cathodic peaks at 3.3 V and 3.1 V (vs. Li/Li^+) correspond to phase changes from α-V_2O_5 to ε-$Li_xV_2O_5$ with subsequent change into δ-$Li_xV_2O_5$ [20,27]. The third cathodic peak at 2.2 V is attributed to the intercalation of the other Li^+ ions, leading to the formation of γ-$Li_xV_2O_5$ [20,27]. Three anodic peaks observed at 2.5, 3.4 and 3.5 V are ascribed to the Li^+ ion de-

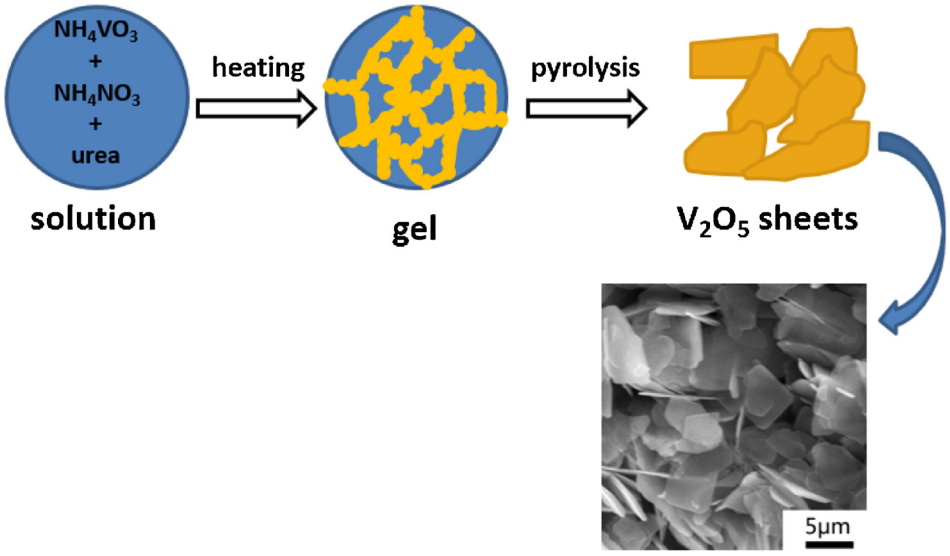

Fig. 4. Illustrations of the preparing V_2O_5 sheets.

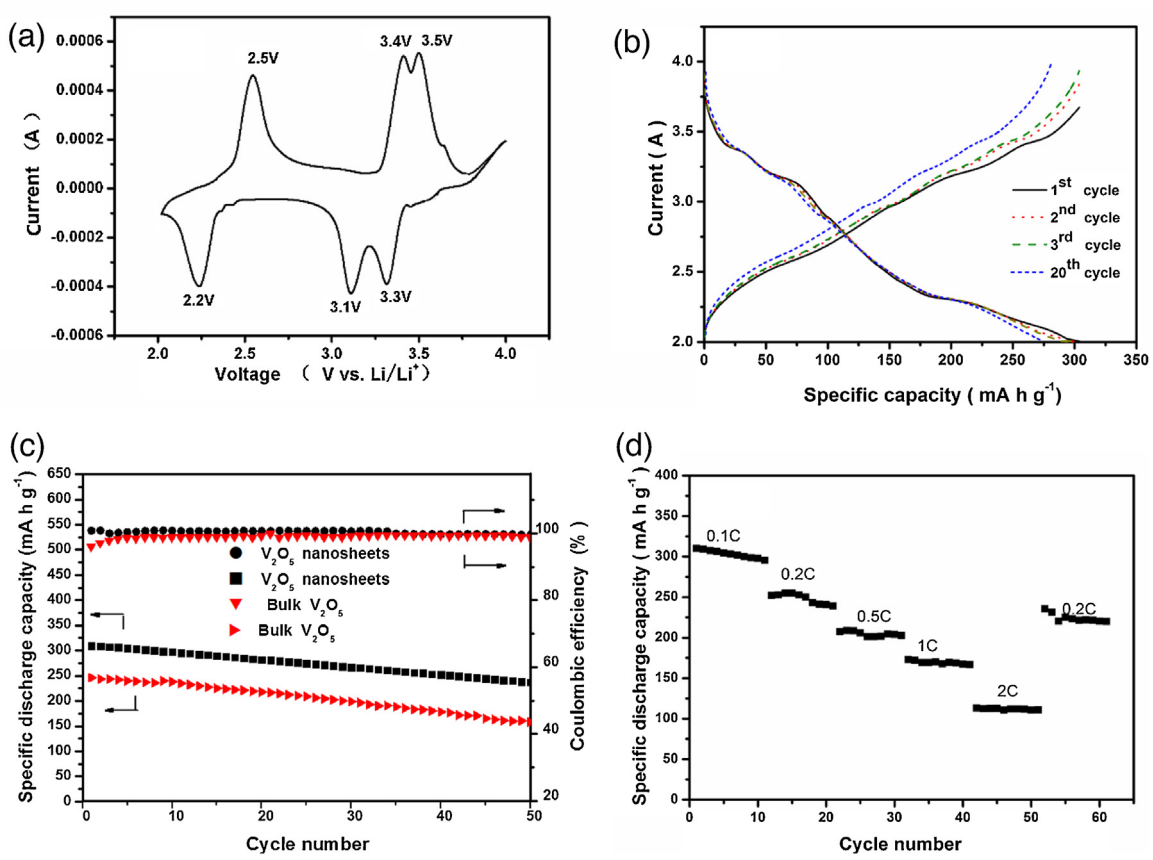

Fig. 5. Electrochemical characterizations of V_2O_5 sheets: (a) Typical CV curve at a scanning rate of 0.2 mV s^{-1}; (b) Galvanostatic charge/discharge curves at 0.1C (29.4 mA g^{-1}); (c) Cycling performance and coulombic efficiency at the current density of 0.1C(29.4 mA g^{-1}); (d) Rate performance.

intercalation process and the corresponding reverse phase transformations from γ-$Li_xV_2O_5$ to δ-$Li_xV_2O_5$, ε-$Li_xV_2O_5$, and α-V_2O_5, respectively [20,27]. The above results demonstrate good reversibility of the crystal structures. Fig. 5b shows the charge-discharge curves of the 1st, 2nd and 3rd cycles at a current density of 29.4 mA g^{-1} (0.1C), which exhibit the specific discharge capacities of 310 mA h g^{-1}, 308 mA h g^{-1} and 307 mA h g^{-1}, respectively. Three plateaus are well observed at 3.3, 3.1 and 2.2 V on the discharge curves, indicating the multi-step Li^+ ion intercalation processes [33]. Three corresponding plateaus related to the Li^+ ion de-intercalation were observed on the charge curves. The plateaus in the discharge and charge curves were all observed upon cycling, demonstrating the good structural reversibility. Fig. 5c presents the cycling performance and coulombic efficiency of the V_2O_5 sheets electrode from the 1st to the 50th cycles at a current density of 29.4 mA g^{-1} (0.1C). The sample delivers high initial discharge capacity of 310 mA h g^{-1}, which is higher than the initial discharge capacity of 248 mA h g^{-1} that can be achieved for the bulk V_2O_5 synthesized by NH_4VO_3 calcination in air at 300 °C. It is mainly suggested that the single crystal sheet facilitates the transport of Li ions, resulting in much shorter diffusion distance for Li ions and electron transport [17]. After 50 cycles, the sheets still retained a reversible capacity of about 234 mA h g^{-1}, corresponding to 75% of the initial capacity. For the voltage windows of 2–4 V, the coulombic efficiency remained close to 100% during the cycling tests, suggesting good reversibility for the lithiation/delithiation process. Fig. 5d shows the rate capability of the V_2O_5 sheets electrode at various current densities. The specific discharge capacities were 309 mA h g^{-1}, 252 mA h g^{-1}, 210 mA h g^{-1}, 172 mA h g^{-1}, and 113 mA h g^{-1} at current densities of 0.1C, 0.2C, 0.5C, 1C, and 2C, respectively. The electrode delivered stable capacities at current densities of 1C and 2C. Furthermore, when the current density decreased from 2C to 0.2C, the capacity was maintained around 230 mA h g^{-1}. Compared with electrochemical performance of other V_2O_5 powders reported in literature [28,34–36], the as-prepared V_2O_5 sheets has better initial discharge capacity, along with improved cyclic retention properties. The well electrochemical performance of the V_2O_5 sheets demonstrates the beneficial effects of the unique sheet structure. The sheet structure not only increases the contact area between the active material and electrolyte, but also greatly facilitates intercalation and deintercalation of Li^+ ions due to the short diffusion length.

4. Conclusions

In summary, a high-performance orthorhombic single crystal V_2O_5 sheets for LIBs was synthesized by a facile one-pot organics-assisted pyrolysis method. The TG-MS measurements revealed the intrinsic pyrolytic reaction mechanism of the as-prepared V_2O_5 sheets. As a cathode materials for LIBs, the V_2O_5 sheets delivered high initial discharge capacity of 310 mA h g^{-1} and the coulombic efficiency remains close to 100% during the 50 charge-discharge cycles. Good electrochemical performance is attributed to the unique single crystal sheets, which facilitate electrolyte penetration, Li^+ ions diffusion and electron transport. Due to the advantages of simple process, low cost and excellent scalability, the facile approach described in this paper is promising for preparing V_2O_5 sheets as high-performance LIBs cathodes.

Acknowledgments

This work was supported by the National Natural Science Foundation Program of China (51574031), the Program for the New Century Excellent Talents in University (NCET-10-0226), and the Fundamental Research Funds for the Central Universities (FRF-TP-11-004A) and the National 863 Program (2013AA031101)

Appendix A. Supplementary data

Supplementary data associated with this article can be found, in the online version, at http://dx.doi.org/10.1016/j.electacta.2016.04.169.

References

[1] J. Livage, Synthesis of polyoxovanadates via “chimie douce”, Coordin Chem Rev 178 (1998) 999–1018.
[2] Y. Xu, M. Dunwell, L. Fei, E. Fu, Q. Lin, B. Patterson, B. Yuan, S. Deng, P. Andersen, H. Luo, Two-Dimensional V_2O_5 Sheet Network as Electrode for Lithium-Ion Batteries, ACS Appl Mater Inter 6 (2014) 20408–20413.
[3] X. Zhang, K. Wang, X. Wei, Carbon-coated V_2O_5 nanocrystals as high performance cathode material for lithium ion batteries, J. Chen. Chem Mater 23 (2011) 5290–5292.
[4] J. Liu, H. Xia, D. Xue, L. Lu, Double-shelled nanocapsules of V_2O_5-based composites as high-performance anode and cathode materials for Li ion batteries, J Am Chem Soc 131 (2009) 12086–12087.
[5] A. Pan, H.B. Wu, L. Yu, X.W.D. Lou, Template-free synthesis of VO_2 hollow microspheres with various interiors and their conversion into V_2O_5 for lithium-ion batteries, Angewandte Chemie 125 (2013) 2282–2286.
[6] M. Sasidharan, N. Gunawardhana, M. Yoshio, K. Nakashima, V_2O_5 hollow nanospheres: A lithium intercalation host with good rate capability and capacity retention, J Electrochem Soc 159 (2012) A618–A621.
[7] Y. Tang, X. Rui, Y. Zhang, T.M. Lim, Z. Dong, H.H. Hng, X. Chen, Q. Yan, Z. Chen, Vanadium pentoxide cathode materials for high-performance lithium-ion batteries enabled by a hierarchical nanoflower structure via an electrochemical process, J Mater Chem A 1 (2013) 82–88.
[8] Y. Wang, H.J. Zhang, K.W. Siah, C.C. Wong, J. Lin, A. Borgna, One pot synthesis of self-assembled V_2O_5 nanobelt membrane via capsule-like hydrated precursor as improved cathode for Li-ion battery, Journal of Materials Chemistry 21 (2011) 10336–10341.
[9] D. Yu, C. Chen, S. Xie, Y. Liu, K. Park, X. Zhou, Q. Zhang, J. Li, G. Cao, Mesoporous vanadium pentoxide nanofibers with significantly enhanced Li-ion storage properties by electrospinning, Energ Environ Sci 4 (2011) 858–861.
[10] L. Cao, J. Zhu, Y. Li, P. Xiao, Y. Zhang, S. Zhang, S. Yang, Ultrathin single-crystalline vanadium pentoxide nanoribbon constructed 3D networks for superior energy storage, J Mater Chem A 2 (2014) 13136–13142.
[11] A. Choudhury, J.S. Bonso, M. Wunch, K.S. Yang, J.P. Ferraris, D.J. Yang, In-situ synthesis of vanadium pentoxide nanofibre/exfoliated graphene nanohybrid and its supercapacitor applications, J Power Sources 287 (2015) 283–290.
[12] Y. Wu, G. Gao, G. Wu, Self-assembled three-dimensional hierarchical porous V_2O_5/graphene hybrid aerogels for supercapacitors with high energy density and long cycle life, J Mater Chem A 3 (2015) 1828–1832.
[13] G. Yilmaz, C.X. Guo, X. Lu, High-Performance Solid-State Supercapacitors Based on V_2O_5/Carbon Nanotube Composites, ChemElectroChem (2015).
[14] A. Pan, J. Zhang, Z. Nie, G. Cao, B.W. Arey, G. Li, S. Liang, J. Liu, Facile synthesized nanorod structured vanadium pentoxide for high-rate lithium batteries, Journal of Materials Chemistry 20 (2010) 9193–9199.
[15] T. Watanabe, Y. Ikeda, T. Ono, M. Hibino, M. Hosoda, K. Sakai, T. Kudo, Facile synthesized nanorod structured vanadium pentoxide for high-rate lithium batteries, Solid State Ionics 151 (2002) 313–320.
[16] J. Muster, G.T. Kim, V. Krstić, J.G. Park, Y.W. Park, S. Roth, M. Burghard, Electrical transport through individual vanadium pentoxide nanowires, Adv Mater 12 (2000) 420–424.
[17] X. Rui, Z. Lu, H. Yu, D. Yang, H.H. Hng, T.M. Lim, Q. Yan, Ultrathin V_2O_5 nanosheet cathodes: realizing ultrafast reversible lithium storage, Nanoscale 5 (2013) 556–560.
[18] Y. Su, A. Pan, Y. Wang, J. Huang, Z. Nie, X. An, S. Liang, Template-assisted formation of porous vanadium oxide as high performance cathode materials for lithium ion batteries, J Power Sources 295 (2015) 254–258.
[19] Z. Wang, L. Zhou, Metal Oxide Hollow Nanostructures for Lithium-ion Batteries, Adv Mater 24 (2012) 1903–1911.
[20] Y.L. Cheah, V. Aravindan, S. Madhavi, Electrochemical lithium insertion behavior of combustion synthesized V_2O_5 cathodes for lithium-ion batteries, J Electrochem Soc 159 (2012) A273–A280.
[21] L. Mai, X. Xu, L. Xu, C. Han, Y. Luo, Vanadium oxide nanowires for Li-ion batteries, J Mater Res 26 (2011) 2175–2185.
[22] R. Yu, C. Zhang, Q. Meng, Z. Chen, H. Liu, Z. Guo, Facile synthesis of hierarchical networks composed of highly interconnected V_2O_5 nanosheets assembled on carbon nanotubes and their superior lithium storage properties, ACS Appl Mater Inter 5 (2013) 12394–12399.
[23] J. Liu, X.W. Liu, Two-Dimensional Nanoarchitectures for Lithium Storage, Adv Mater 24 (2012) 4097–4111.
[24] M. Li, G. Sun, P. Yin, C. Ruan, K. Ai, Controlling the Formation of Rodlike V_2O_5 Nanocrystals on Reduced Graphene Oxide for High-Performance Supercapacitors, ACS Appl Mater Inter 5 (2013) 11462–11470.
[25] Q. An, Q. Wei, L. Mai, J. Fei, X. Xu, Y. Zhao, M. Yan, P. Zhang, S. Huang, Supercritically exfoliated ultrathin vanadium pentoxide nanosheets with high rate capability for lithium batteries, Phys Chem Chem Phys 15 (2013) 16828–16833.
[26] J. Cheng, B. Wang, H.L. Xin, G. Yang, H. Cai, F. Nie, H. Huang, Self-assembled V_2O_5 nanosheets/reduced graphene oxide hierarchical nanocomposite as a high-performance cathode material for lithium ion batteries, J Mater Chem A 1 (2013) 10814–10820.
[27] A.Q. Pan, H.B. Wu, L. Zhang, X.W.D. Lou, Uniform V_2O_5 nanosheet-assembled hollow microflowers with excellent lithium storage properties, Energ Environ Sci 6 (2013) 1476–1479.
[28] P. Ragupathy, S. Shivakumara, H.N. Vasan, N. Munichandraiah, Preparation of nanostrip V_2O_5 by the polyol method and its electrochemical characterization as cathode material for rechargeable lithium batteries, The Journal of Physical Chemistry C 112 (2008) 16700–16707.
[29] T. Wanjun, L. Yuwen, Y. Xi, W. Cunxin, Kinetic studies of the calcination of ammonium metavanadate by thermal methods, Ind Eng Chem Res 43 (2004) 2054–2059.
[30] G. Li, Y. Qiu, Y. Hou, H. Li, L. Zhou, H. Deng, Y. Zhang, Synthesis of V_2O_5 hierarchical structures for long cycle-life lithium-ion storage, J Mater Chem A 3 (2015) 1103–1109.
[31] Z. Xingfu, H. Zhaolin, F. Yiqun, C. Su, D. Weiping, X. Nanping, Microspheric organization of multilayered ZnO nanosheets with hierarchically porous structures, The Journal of Physical Chemistry C 112 (2008) 11722–11728.
[32] T. Xiao, Y. Tang, Z. Jia, D. Li, X. Hu, B. Li, L. Luo, Self-assembled 3D flower-like Ni^{2+}-Fe^{3+} layered double hydroxides and their calcined products, Nanotechnology 20 (2009) 475603.
[33] H.G. Wang, D.L. Ma, Y. Huang, X.B. Zhang, Electrospun V_2O_5 Nanostructures with Controllable Morphology as High-Performance Cathode Materials for Lithium-Ion Batteries, Chem-Eur J 18 (2012) 8987–8993.
[34] Y.L. Cheah, N. Gupta, S.S. Pramana, V. Aravindan, G. Wee, M. Srinivasan, Morphology: structure and electrochemical properties of single phase electrospun vanadium pentoxide nanofibers for lithium ion batteries, J Power Sources 196 (2011) 6465–6472.
[35] L. Mai, L. Xu, C. Han, X. Xu, Y. Luo, S. Zhao, Y. Zhao, Electrospun ultralong hierarchical vanadium oxide nanowires with high performance for lithium ion batteries, Nano Lett 10 (2010) 4750–4755.
[36] D. Zhu, H. Liu, L. Lv, Y.D. Yao, W.Z. Yang, Hollow microspheres of V_2O_5 and Cu-doped V_2O_5 as cathode materials for lithium-ion batteries, Scripta Mater 59 (2008) 642–645.